BIOCHEMISTRY
including biophysical chemistry & molecular biology

Article

pubs.acs.org/biochemistry

Structure and Catalytic Mechanism of Nicotinate (Vitamin B_3) Degradative Enzyme Maleamate Amidohydrolase from *Bordetella bronchiseptica* RB50

Virginia A. Kincaid,[†] Eric D. Sullivan,[†] Roger D. Klein,[†] Jeff W. Noel,[†] Roger S. Rowlett,[‡] and Mark J. Snider*,[†]

[†]Department of Chemistry, The College of Wooster, Wooster, Ohio 44691, United States

[‡]Department of Chemistry, Colgate University, Hamilton, New York 13346, United States

Supporting Information

ABSTRACT: The penultimate reaction in the oxidative degradation of nicotinate (vitamin B_3) to fumarate in several species of aerobic bacteria is the hydrolytic deamination of maleamate to maleate, catalyzed by maleamate amidohydrolase (NicF). Although it has been considered a model system for bacterial degradation of N-heterocyclic compounds, only recently have gene clusters that encode the enzymes of this catabolic pathway been identified to allow detailed investigations concerning the structural basis of their mechanisms. Here, the *Bb*1774 gene from *Bordetella bronchiseptica* RB50, putatively annotated as *nicF*, has been cloned, and the recombinant enzyme, overexpressed and purified from *Escherichia coli*, is shown to catalyze efficiently the hydrolysis of maleamate to maleate and ammonium ion. Steady-state kinetic analysis of the reaction by isothermal titration calorimetry (ITC) established k_{cat} and K_M values (pH 7.5 and 25 °C) of 11.7 ± 0.2 s^{-1} and 128 ± 6 μM, respectively. The observed K_D of the NicF·maleate (E·P) complex, also measured by ITC, is approximated to be 3.8 ± 0.4 mM. The crystal structure of NicF, determined at 2.4 Å using molecular replacement, shows that the enzyme belongs to the cysteine hydrolase superfamily. The structure provides insight concerning the roles of potential catalytically important residues, most notably a conserved catalytic triad (Asp29, Lys117, and Cys150) observed in the proximity of a conserved non-proline *cis*-peptide bond within a small cavity that is likely the active site. On the basis of this structural information, the hydrolysis of maleamate is proposed to proceed by a nucleophilic addition−elimination sequence involving the thiolate side chain of Cys150.

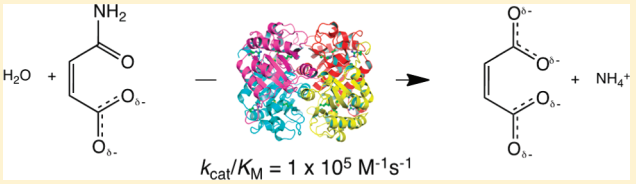

Nicotinate (niacin, vitamin B_3) serves as the source of the nicotinamide moiety of NAD^+ and $NADP^+$, coenzymes central to metabolism in all living species. Nicotinate can also serve as a source of carbon, nitrogen, and energy for a variety of bacteria[1−5] (for reviews, see refs 6 and 7), and its catabolism can occur by multiple routes, depending on oxygen availability, in which 6-hydroxynicotinate is the common first intermediate.[8,9] Microbial degradation of nicotinate is considered a model pathway for enzymatic degradation of N-heterocyclic aromatic compounds in the environment.[7] The genes that encode the enzymes of these degradation pathways have been shown[10,11] to exist in bacteria that inhabit soil rhizhospheres (e.g., *Pseudomonas* sp., *Burkholderia xenovorans*, and *Eubacterium barkeri*), in which plants are a significant source of nicotinate in the environment, and in pathogenic bacteria (e.g., *Bordetella*) that infect the respiratory tract of animals. It is of interest to note that nicotinate has been shown to modulate virulence factor expression in *Bordetella pertussis*,[12−14] the causative agent of whooping cough, suggesting that a more comprehensive understanding of the biochemical details of the enzymes of nicotinate catabolism may also be of pharmaceutical value.

An aerobic degradation pathway for nicotinate (Figure 1) was originally characterized biochemically by Behrman and Stanier.[15] In that study, 6-hydroxynicotinate (**2**) is shown to be oxidized to 2,5-dihydroxypyridine (**3**), which is subsequently transformed to maleamate (**5**) through a dioxygenase-catalyzed ring-opening reaction proposed[15,16] to proceed through *N*-formylmaleamate (**4**) as an intermediate. The existence of that intermediate has been confirmed.[11] After hydrolytic deformylation, maleamate undergoes hydrolysis to maleate (**6**), which is then isomerized to fumarate (**7**), a common intermediate in central metabolism. The recent determination of the complete nicotinate catabolizing gene cluster in *Pseudomonas putida*[11] has provided the potential for structural and more detailed mechanistic studies of the enzymes from this pathway.

Maleamate amidohydrolase (NicF, EC 3.5.1.107) catalyzes the hydrolysis of the amide bond in maleamate to form maleate and ammonium ion [**5** to **6** (Figure 1)] in the penultimate reaction of the degradation of nicotinate to fumarate. The *nicF* gene in *P. putida* was originally identified[11] on the basis of its

Received: August 25, 2011
Revised: November 23, 2011
Published: December 23, 2011

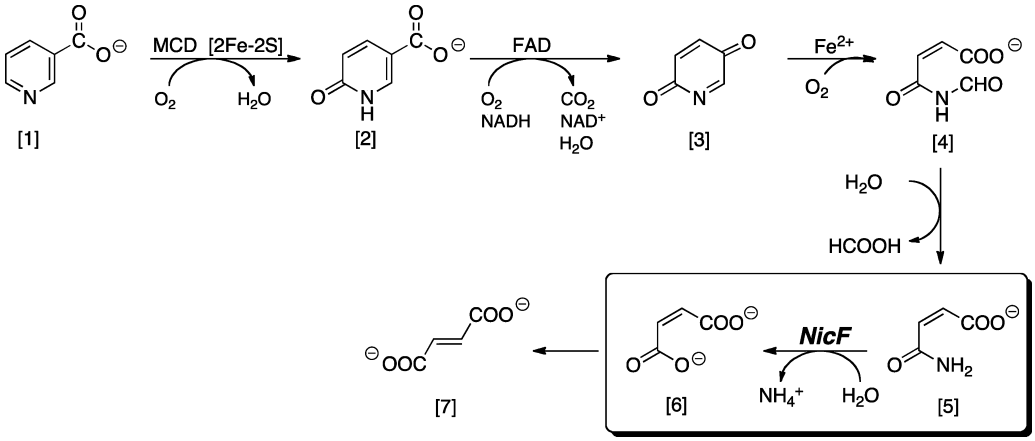

Figure 1. Aerobic pathway for bacterial nicotinate catabolism established in *Pseudomonas fluorescens*.[15] Nicotinate (**1**) is oxidized to 6-hydroxynicotinate (**2**, 6-HNA) by a two-component Fe_2S_2 cluster and molybdopterin cytosine dinucleotide (MCD)-dependent hydroxylase (NicAB).[11] 6-HNA is then oxidized to 2,5-dihydroxypyridine (**3**) by a flavin-dependent monooxygenase (NicC). Ring-opening oxidation of **3** to *N*-formylmaleamate (**4**) is catalyzed by an Fe^{2+}-dependent dioxygenase (NicX). Hydrolysis of **4** to maleamate (**5**) is catalyzed by a hydrolytic deformylase (NicD). Hydrolytic deamination of **5** to maleate (**6**) is catalyzed by maleamate amidohydrolase (NicF). Conversion of the *Z* isomer of **6** to its *E* isomer, fumarate (**7**), is catalyzed by maleate isomerase (NicE).

sequence similarity to members of the isochorismatase superfamily, which includes *N*-carbamoylsarcosine amidohydrolase (CSHase)[17] and nicotinamidase,[18,19] enzymes that also catalyze amide bond hydrolysis of their cognate substrates. Although earlier work demonstrated NicF activity in soluble *Pseudomonas* extracts,[11,15] no studies to date have provided information concerning a kinetic or structural mechanism of its action. Here we demonstrate that the *Bb*1774 gene, previously annotated as an *N*-carbamoylsarcosine amidase, is instead a catalytically efficient maleamate amidohydrolase that is part of a putative *nic* cluster in *Bordetella bronchiseptica* RB50. The crystal structure reported here provides structural evidence of a mechanistic proposal involving nucleophilic catalysis by Cys150.

MATERIALS AND METHODS

Molecular Cloning. Standard methods were used for DNA manipulations.[20] Plasmid DNA was purified with the Fermentas GeneJET Plasmid Miniprep Kit, and DNA fragments, produced by digestion with *Nde*I and *Xho*I (New England Biolabs), were purified from a 1% (w/v) agarose gel with the Zymoclean Gel DNA Recovery Kit. *Escherichia coli* strain MachI (Invitrogen) was used as the recipient for transformations during plasmid construction and propagation. Phusion DNA polymerase (New England Biolabs) was used for polymerase chain reaction (PCR) following the manufacturer's recommended protocols.

The *Bb*1774 gene of *B. bronchiseptica* was amplified from the genomic DNA (ATCC BAA-588D) by PCR with the following primers: 5′-GGTAG CAT ATG GGC AAT GAT CTG GGC AGC TAC GAG CGC-3′ and either 5′-GGTAG CTC GAG TCA CTT TGT CTT TGC CAG CGC CTC GTC ATG CGT C-3′ to express His_6-NicF or 5′-GGTAG CTC GAG TCC CTT TGT CTT TGC CAG CGC CTC GTC ATG CGT C-3′ to replace the native stop codon in *nicF* with a Gly codon to permit expression of His_6-NicF-His_6. PCR products were gel purified and individually ligated into the pTHT protein expression plasmid (Cornell University Protein Facility), a vector based on the pET system. The pTHT plasmid encodes an N-terminal tag GSDKIHHHHHHSSGENLYFQ∧GH (where the ∧ marks the tobacco etch virus, TEV, protease cleavage site) and a C-terminal tag GLEHHHHHH, in which protein expression is under control of the T7*lac* promoter. Clones were screened by restriction digestion and verified by DNA sequencing, performed at the Molecular & Cellular Imaging Facility at the Ohio Agricultural Research & Development Center of The Ohio State University, using the standard T7 primer.

Overexpression and Purification. *E. coli* BL21(DE3) cells (Novagen) were transformed with the pTHT_nicF plasmid and grown overnight at 37 °C on LB plates containing kanamycin (50 μg/mL). A single colony was used to inoculate a 10 mL starter culture of LB containing kanamycin (50 μg/mL) for overnight growth at 37 °C with agitation, which was subsequently used to inoculate 1.0 L of LB medium supplemented with kanamycin (50 μg/mL) and $MgSO_4$ (2.0 mM). The cells were then shaken at 37 °C until the culture reached an OD_{600} of 1.0−1.2, at which point protein expression was induced by the addition of sterile IPTG to a final concentration of 1.0 mM. The culture was transferred to a shaker at 18 °C and allowed to express protein for an additional 12−15 h. The cells were then harvested by centrifugation at 8000*g* for 15 min at 4 °C.

Cells (~6−8 g of wet weight) from 1 L of culture were resuspended in 40 mL of ice-cold binding buffer [50 mM NaH_2PO_4 (pH 8.0), 300 mM NaCl, 40 mM imidazole, and 1 mM DTT]. Cell lysis was achieved by sonication with a 1.0 s intermittent pulse time for 1 min, repeated six to eight times. The temperature of the lysis solution was kept below 10 °C for the duration of the sonication. The cellular debris was removed by centrifugation at 15000*g* for 30 min at 4 °C. The clarified supernatant was loaded onto a 5.0 mL HisTrap HP column (GE Life Sciences) pre-equilibrated with binding buffer at 4 °C using an ÄKTA fast performance liquid chromatography (FPLC) system. The loaded column was washed with 15 column volumes of binding buffer, and the His_6-tagged NicF protein was then eluted with a gradient (10% elution buffer per minute) using elution buffer [50 mM NaH_2PO_4 (pH 8.0), 300 mM NaCl, 500 mM imidazole, and 1 mM DTT]. Fractions containing the protein were pooled and concentrated using YM-10 Amicon ultrafiltration filters (10 kDa molecular mass cutoff) at 5000*g* to a final volume of 3 mL. The concentrated samples were desalted and exchanged into storage buffer [10

mM Tris (pH 7.2), 100 mM NaCl, 0.1 mM EDTA, and 25% (v/v) glycerol] using an Econo-Pac 10DG column (Bio-Rad) pre-equilibrated in storage buffer. Protein concentrations were determined by the absorbance at 280 nm, using molar absorptivity coefficients (e.g., 21430 M^{-1} cm^{-1} for His_6-NicF) calculated by the method of Pace et al.[21] Aliquots (100 μL) of concentrated protein (~15 mg/mL) were flash-frozen in liquid N_2 and stored at −80 °C.

To determine whether the N- or C-terminal His_6 tags affected NicF activity, each recombinant enzyme was purified. The NicF enzyme was produced by removal of the N-terminal His_6 of His_6-NicF, and the NicF-His_6 enzyme was produced by removal of the N-terminal His_6 of His_6-NicF-His_6. Removal of the His_6 tags was accomplished by incubation with TEV protease in sodium phosphate buffer (100 mM, pH 7.5) containing DTT (1 mM) for 3 days at 4 °C. Any remaining His_6-NicF protein after reaction with TEV protease was removed by applying the reaction mixture to a Ni^{2+} Sepharose fast flow column (New England Biolabs), to which the NicF protein does not bind. Analysis of the TEV reaction by SDS−PAGE showed that the reactions had gone nearly to completion. Specific activities of the His_6-NicF-His_6, His_6-NicF, NicF-His_6, and NicF enzymes were compared, using the assays described below. The uncleaved His_6-NicF-His_6 recombinant enzyme was used in the crystallography experiments.

^{1}H Nuclear Magnetic Resonance (NMR) Analysis of the NicF Reaction Product. NicF (0.5 mg) was incubated with maleamate (10 mM) in sodium phosphate buffer (100 mM, pH 7.5) at room temperature for 30 min. An aliquot of this reaction mixture (100 μL) was added to 900 μL of D_2O in which pyrazine (1 mM) was included as a chemical shift standard. The ^{1}H NMR spectrum (400 MHz) was acquired (ns = 8; D_1 = 1.00 s) and compared to the ^{1}H NMR spectra of maleamate and maleate (Sigma Aldrich) standards, prepared separately at final concentrations of 1 mM in D_2O following the same procedures outlined above, except for the addition of enzyme.

Assay for Ammonia. The assay for product ammonia and the initial steady-state kinetic characterization of NicF activity were conducted by monitoring the disappearance of NADPH (followed at 340 nm; $\Delta\varepsilon$ = 6200 M^{-1} cm^{-1}) with time in a coupled assay with glutamate dehydrogenase.[22] The assay mixture (1.0 mL) contained glutamate dehydrogenase (10 units), α-ketoglutarate (10 mM), EDTA (1 mM), NADH (250 μM), NicF (160 nM), and maleamate (ranging from 50 to 750 μM) in sodium phosphate buffer (100 mM, pH 7.4) at 25 °C. The reduction of α-ketoglutarate to glutamate was determined not to be rate-limiting under these conditions, and rates of background NADPH oxidation (assays lacking maleamate) were determined to be less than 10% of the desired reaction rate.

Steady-State Kinetic Analysis by Isothermal Titration Calorimetry. Direct determination of the steady-state kinetic parameters, k_{cat} and K_M, of NicF was achieved by isothermal titration calorimetry (VP-ITC, Microcal) using the multiple-injection method described by Todd and Gomez.[23] Isothermal calorimetric rate measurements were accomplished by measuring the thermal power (dQ/dt) generated by NicF upon addition of aliquots (5−30 μL) of maleamate using eq 1:

$$\text{rate} = \frac{d[P]}{dt} = \frac{1}{V\Delta H_{app}}\frac{dQ}{dt} \quad (1)$$

where V is the volume (1.462×10^{-3} L) of the reaction cell containing the enzyme, ΔH_{app} is the experimentally determined molar enthalpy change for the reaction, and dQ/dt is the change in heat measured with time, measured directly by the displacement of baseline power with each injection of substrate. ΔH_{app} was determined from a separate experiment in which the integration of the heat released upon complete conversion of maleamate to maleate was achieved rapidly in the cell containing NicF (2.25 μM), because the equilibrium favors maleate formation. The solution of maleamate (2.5 mM in the injection syringe) was made using the same buffer [100 mM bicine (pH 7.5)] in which the protein was dialyzed overnight at 4 °C, and the pH was readjusted to 7.5 by addition of NaOH. After thermal equilibrium was reached at 25 °C, maleamate (5 μL) was injected into the cell, giving a final maleamate concentration of 9 μM. After equilibrium had been re-established (~5 min), additional aliquots (5 μL each) of maleamate were injected. Under these conditions, numerical integrations of the area under each independent peak were observed to match closely, producing an apparent enthalpy of reaction (ΔH_{app}) of −9.17 ± 0.02 kcal/mol (Figure S1 of the Supporting Information).

To measure the steady-state rate of maleate formation, we measured the baseline thermal power for several minutes prior to the first injection of maleamate (2.5 mM in the syringe) into the reaction cell containing NicF (5.6 nM) in which the reaction buffers [100 mM bicine (pH 7.5)] matched. As soon as the displacement of baseline power had reached a new plateau, the next aliquot of maleamate was added before the reaction could return to the original baseline (i.e., reach equilibrium). In this way, it can be assumed that the added maleamate is not significantly turned over to product during each injection so that its concentration for each injection can be calculated from a summation of all prior injections. Calorimetric rates were measured at the following maleamate concentrations (final, in the cell): 10.2, 18.7, 27.2, 35.7, 44.1, 52.5, 69.1, 85.7, 102, 151, 198, 245, 290, 335, and 378 μM.

Rates from both the ammonia assay, established from linear regression analyses of initial rates of NADPH oxidation in the GDH-coupled assay, and direct isothermal titration calorimetry were fit individually to the Michaelis−Menten equation (eq 2) using nonlinear regression analysis (KaleidaGraph version 4.02) to give the kinetic constants for NicF-catalyzed maleamate hydrolysis.

$$\text{rate} = \frac{k_{cat}[E]_T[S]}{K_M + [S]} \quad (2)$$

Inactivation by Iodoacetamide. Two solutions [bicine (50 mM) and TCEP (2 mM) (pH 7.5)] containing NicF (300 μM), one with iodoacetamide (3.0 mM), were incubated for 90 min at room temperature. An aliquot (60 μL) was removed from each and applied to separate Micro Bio-Spin columns (Bio-Rad), equilibrated in the same reaction buffer, and centrifuged following the manufacturer's instructions to remove unreacted iodoacetamide. Eluent from each column was added to separate reaction buffers [50 mM bicine (pH 7.5); 2 mM TCEP] to dilute the NicF to a final concentration of 5.6 nM. The activity of each sample was measured for NicF activity

using isothermal titration calorimetry following the procedure described previously.

Binding of Maleate by NicF. The apparent dissociation constant (K_D) of the maleate·NicF complex was measured by ITC. NicF was dialyzed overnight [100 mM bicine (pH 7.5) containing 2 mM TCEP] at 4 °C, and the dialysis buffer was used to make a solution of maleate. After thermal equilibration was reached at 25 °C, aliquots of the maleate solution (18 mM) were injected into the cell containing NicF (716 μM), allowing baseline equilibration to be achieved between injections. The heat evolved after each injection was obtained from the integrated intensity of the calorimetric signal. Integration and nonlinear least-squares analysis of the data using a single-binding site model, in which the number of binding sites was set to 1, were accomplished using Origin (version 7, Microcal). Thermodynamic values are the average of two experiments.

Inhibition of NicF by maleate (4.0 mM) was measured using the multi-injection isothermal titration calorimetric method described above, using 5.6 nM NicF with varying concentrations of maleamate, in PIPES-buffered solutions (50 mM, pH 7.5) at 25 °C.

Detection of Zinc. The quantity of Zn^{2+} in NicF was measured by flame atomic absorption spectroscopy (Thermo S Series) using an air-acetylene flame. A stock solution of $ZnCl_2$ was made by dissolving 50.0 mg of $ZnCl_2$ in 5.00 mL of aqueous HNO_3 (2 M). Standards of $ZnCl_2$ from this stock solution were made fresh in 5.00 mL of a glycerol (5%, v/v) solution with final Zn^{2+} concentrations of 0.0050, 0.010, 0.020, 0.100, and 0.200 μg/mL. Absorbance measurements were recorded in triplicate at 213.9 nm using a Thermo 10 mA Zn hollow cathode lamp. Purified His_6-NicF was also diluted in 5 mL of a glycerol (5%, v/v) solution to a final concentration of 0.10 μg/mL and aspirated into the AA spectrometer, and the absorbance at 213.9 nm was recorded in triplicate.

Protein Quaternary Structure. The apparent molecular weight of the enzyme was determined by gel exclusion chromatography in 50 mM sodium phosphate (pH 7.00), 150 mM NaCl, and 5 mM DTT, using a calibrated 2.6 cm × 60 cm Sephacryl S-200 column (GE Life Sciences) at a flow rate of 0.75 mL/min at 4 °C using an AKTA FPLC system (GE Life Sciences). NicF and the set of standards were individually injected as 100 μL aliquots, and elution was monitored by absorbance at 280 nm. The following calibration standards were used: γ-globulin (158 kDa), ovalbumin (44 kDa), and myoglobin (17 kDa) (from Bio-Rad) and alchohol dehydrogenase (150 kDa), albumin (66 kDa), carbonic anhydrase (29 kDa), and cytochrome *c* (12.4 kDa) (from Sigma-Aldrich).

Protein Crystallization. The hanging drop vapor diffusion method was used with 1 μL of a His_6-NicF-His_6 protein solution (15 mg/mL in storage buffer) and 1 μL of reservoir solution (500 μL) at room temperature (~22 °C). Sparse matrix screens were used to determine initial hits (Crystal Screen, Hampton Research), and diffraction quality crystals (0.3−0.4 mm in diameter) grew within 3 weeks directly from initial Hampton Research Crystal Screen formulation 15 [0.2 M ammonium acetate, 0.1 M sodium cacodylate trihydrate (pH 6.5), and 30% (w/v) PEG 8000]. Crystals were cryoprotected by being transferred into artificial mother liquor supplemented with D-glucose (25%, w/v) for 1−2 min and then flash-cooled in liquid nitrogen.

X-ray Data Collection and Processing. Data collection was performed with an Oxford Diffraction Gemini R system using a PX Ultra Enhance Cu Kα source and a Ruby CCD detector. Diffraction data to 2.40 Å resolution were collected using 120 s frames and a 0.3° scan width. Space group assignment, data integration, and scaling were performed with CrysalisPro.[24] The crystal belonged to space group *R*3 (*H*3) with the following unit cell parameters: $a = b = 157.6$ Å, and $c = 198.5$ Å.

Molecular replacement phasing using unmodified sequence-related proteins was not successful. Phasing was accomplished by molecular replacement using a modified search model derived from *N*-carbamoylsarcosine amidohydrase [Protein Data Bank (PDB) entry 1NBA][17] followed by extensive density modification, noncrystallographic symmetry averaging, and automated chain building. Briefly, the sequence of NicF (minus tag sequences) was submitted to the Phyre[25] server to generate a monomer with the *NicF* sequence based on the three-dimensional structure of 1NBA. Pymol[26] was used to generate and align a second copy of the Phyre model with chain B of 1NBA to construct a dimer. This dimer was used as a search model in Phaser.[27−29] The Phaser solution had reasonable solvent content and protein chain packing in the unit cell, with few clashes. Four dimers were found in the asymmetric unit, with a solvent content of 55.43% and a Matthews coefficient of 2.78 Å^3/Da. While the electron density map was reasonably interpretable, the solution was clearly misregistered to the electron density data in many areas, resulting in an *R* of 0.44 and a figure of merit (FOM) of 0.34 after refinement in Refmac.[30]

The Phaser solution was stripped to a poly-Ala sequence using Chainsaw[31] (CCP4), and this model was refined in Refmac[30] with tight NCS to generate better phases. This model and phase data were subjected to 10 rounds of density modification in Parrot,[32] using 8-fold symmetry (NCS) averaging, and the solvent content fraction estimated from Phaser. Parrot improved the FOM to 0.77. Phases obtained from Parrot were fed into Buccaneer[33] for five rounds of automated model building using the full native sequence of NicF, NCS averaging, and stringent probability requirements for sequence matching. The final Buccaneer model had an *R* of 0.31 and a FOM of 0.85. Electron density maps from this solution were readily interpretable.

The autotraced Buccaneer solution was rebuilt in Coot[34] using an NCS-averaged electron density map on chain A. Clearly interpretable electron density for residues 5−205 was observed in the averaged map. Any remaining sequence misregistrations were corrected in Coot, and the rebuilt A chain was copied to chains B−H for 10 rounds of refinement with tight NCS constraints in Refmac, resulting in an *R* of 0.296 and an R_{free} of 0.309. NCS constraints were released, and multiple rounds of rebuilding in Coot resulted in an *R* of 0.255 and an R_{free} of 0.305. This solution could not be improved further, and twinning was suspected. Refinement in Refmac with the TWIN option revealed a twin fraction of 38.7% with a twin operator of $-h\ -k,\ k,\ -l$. Twin refinement in Refmac resulted in a rapid improvement of the model to an *R* of 0.140 and an R_{free} of 0.183, and a significant improvement in electron density. Solvent was added in two rounds of refinement with TLS,[35,36] with one TLS group per protein chain, resulting in the final model. Data collection and refinement statistics are listed in Table 1.

RESULTS

Protein Purification and Oligomerization. The two forms of recombinant His-tagged protein (His_6-NicF and His_6-

Table 1. Data Collection and Refinement Statistics for Maleamate Amidohydrolase (PDB entry 3UAO)[a]

Data Collection	
source	Oxford Enhance Ultra
wavelength (Å)	1.54
space group	*R*3 (*H*3)
cell parameters (Å)	$a = b = 157.6$ Å, $c = 198.5$ Å
resolution (Å)	12.01−2.40 (2.52−2.40)
no. of unique reflections	69904
redundancy	2.2 (1.2)
completeness	97.1 (82.7)
R_{sym} (%)	0.087 (0.271)
$\langle I\rangle/\langle\sigma I\rangle$[b]	15.1 (3.8)
Refinement	
no. of reflections in test set	1400
R_{work} (%)	0.127
R_{free} (%)	0.172
no. of atoms	
protein	11740
ligand	6
ion	64
solvent	576
root-mean-square deviation from ideal[c]	
bond distances (Å)	0.017
bond angles (deg)	1.626
Ramachandran plot outliers (%)[d]	0.0

[a]Values in parentheses represent data for the highest-resolution shell. [b]Reported as $\langle\langle I\rangle/\sigma\langle I\rangle\rangle$ in SCALA. [c]Ideal values from ref 52. [d]Calculated using a strict boundary Ramachandran plot.[53]

NicF-His_6) were overexpressed from BL21(DE3) *E. coli* and successfully purified using Ni^{2+} affinity chromatography. Typical yields of ∼75 mg of protein per liter of cells were obtained at >98% purity as estimated by SDS−PAGE analysis. Gel filtration chromatography measurements with His_6-NicF reveal an apparent enzyme molecular mass of 86 kDa, consistent with a homotetramer (96.4 kDa) calculated from the enzyme sequence.

Product Characterization. Because the *Bb*1774 gene from *B. bronchiseptica* RB50 is annotated as *N*-carbamoylsarcosine amidase, we initially sought to verify NicF activity in the recombinant protein. The carbon-bound hydrogen atoms of maleamate [δ 6.35 (d, J = 12.3 Hz, 1H, H_a), 5.89 (d, J = 12.3 Hz, 1H, H_b)] and maleate [δ 5.96 (s, 2H, H_c)], in which the chemical shifts are set relative to pyrazine [δ 8.60 (4H)] in D_2O, are distinguished readily by ^1H NMR (400 MHz). Spectroscopic analysis of a reaction mixture containing maleamate and the purified recombinant enzyme by ^1H NMR showed only a singlet at 5.95 ppm in that region of the spectrum (Figure S2 of the Supporting Information), providing unequivocal evidence of the formation of maleate from maleamate by the recombinant enzyme.

To provide further evidence of the recombinant enzyme's ability to catalyze the hydrolysis of maleamate to maleate, a standard coupled assay with glutamate dehydrogenase was utilized to detect the production of ammonia by UV absorbance measurements at 340 nm. In the presence of ammonia and α-ketoglutarate, α-iminoglutarate is formed and subsequently reduced, with concomitant oxidation of NADPH, to glutamine. When the coupled enzyme reactions are optimized, the rate of ammonia production is measured directly from the rate of the decrease in absorbance. Under these conditions, a decrease at 340 nm was observed when the coupled assay included recombinant purified enzyme and maleamate; no decrease in absorbance was observed in the absence of maleamate (Figure S3 of the Supporting Information). These results confirmed the production of ammonia during the enzymatic hydrolysis of maleamate and, in combination with structural identification of maleate as the product by NMR, provided conclusive evidence that the *Bb*1774 gene encodes a catalytic NicF.

Enzyme Kinetics. To determine whether the enzyme from *B. bronchiseptica* catalyzed the hydrolysis of maleamate at a physiologically relevant rate and to provide a measure of the steady-state rate constants of the reaction, kinetic analyses of the recombinant purified NicF were performed. Nonlinear fits of the rate of ammonia production by the coupled assay for ammonia as a function of maleamate concentration (50−750 μM) to the Michaelis−Menten equation (Figure S3 of the Supporting Information) estimated a k_{cat} of 18.4 ± 0.3 s^{-1} and a K_M for maleamate of 107 ± 7 μM (pH 7.4, 25 °C). Rates of maleamate hydrolysis catalyzed by His_6-NicF-His_6, His_6-NicF, and NicF (which included an extra GH on the N-terminus of the native sequence as a remnant of the TEV protease recognition site) matched within experimental error, demonstrating that the presence of the purification tags does not affect enzyme activity.

Using the multiple-substrate injection technique described by Todd and Gomez,[23] a robust and reproducible methodology for measuring the steady-state kinetic parameters of NicF was achieved by following the heat released upon maleamate hydrolysis as a function of time and maleamate concentration (10−378 μM). Nonlinear fits to the rate data obtained by ITC to the Michaelis−Menten equation (Figure 2) estimated a k_{cat} of 11.7 ± 0.2 s^{-1} and a K_M of 128 ± 6 μM (pH 7.5, 25 °C), in satisfactory agreement with the results obtained by the coupled enzyme assay for ammonia. Taken together, these results provide a measure of the catalytic efficiency of NicF [k_{cat}/K_M = (9.1 ± 0.5) × 10^4 M^{-1} s^{-1}].

No Role for Zn^{2+} in Catalysis by NicF. Several members of the cysteine amidase family require metal ions for activity, notably Zn^{2+} by PhPZase (see, for example, ref 18) and CSHase from *Thermoplasma acidophilum*.[37] Flame atomic absorption spectroscopy was used to explore the possibility of coordination of Zn^{2+} by NicF. Compared to a set of Zn^{2+}-containing solutions (0.0050−0.2000 μg/mL), which resulted in a satisfactory linear correlation of absorbance (213.9 nm) versus zinc concentration (R^2 = 0.99), no absorbance was observed in a solution containing active His_6-NicF (0.10 μg/mL). In addition, rates of maleamate hydrolysis between His_6-NicF preincubated in bicine-buffered solution (50 mM, pH 7.5, 1 mM DTT, 5% glycerol) containing NaCl (40 mM) or $ZnCl_2$ (40 mM), and then dialyzed in reaction buffer containing no salt, matched. Finally, there is no observable electron density corresponding to a metal ion in the X-ray structure of NicF (vide infra). Thus, the functional data are in accord with structural observations and indicate that, unlike several of its apparent homologues, NicF structure and activity do not depend on Zn^{2+}.

Thermodynamic Analysis of Maleate (Product) Binding by NicF. Maleate binding by NicF, measured by ITC, was found to be only slightly exothermic, yielding a ΔH of −0.50 ± 0.03 kcal/mol after taking into account the heat for dilution of ligand after saturation had been achieved (Figure 3). A nonlinear fit of the titration data using a single-binding site

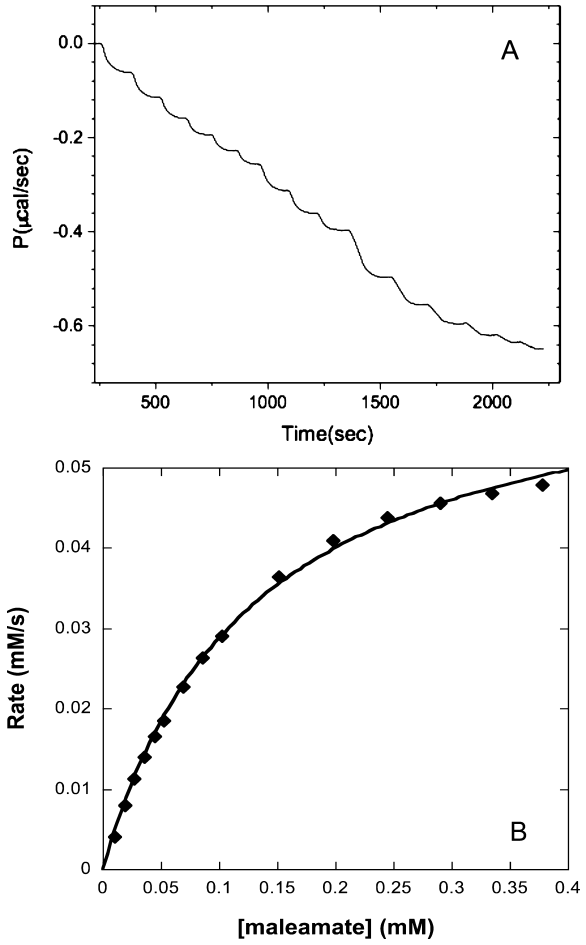

Figure 2. Isothermal calorimetric rate measurements of maleamate hydrolysis catalyzed by NicF. (A) Thermal power required to maintain isothermal conditions upon multiple injections of maleamate (syringe concentration of 2.5 mM) into NicF (initial cell concentration of 5.6 nM) in a bicine-buffered solution (100 mM, pH 7.5) at 25 °C. Conversion of the change in thermal power (dQ/dt) at each new baseline achieved after each injection of substrate to the rate of reaction was accomplished using eq 1, in which $\Delta H_{app} = -9.17 \pm 0.02$ kcal/mol. (B) Nonlinear regression analysis of the rate vs maleamate concentration produces the best fit line ($R = 0.9993$) with a k_{cat} of 11.7 $\pm$ 0.2 s^{-1} and a K_M of 128 $\pm$ 6 μM.

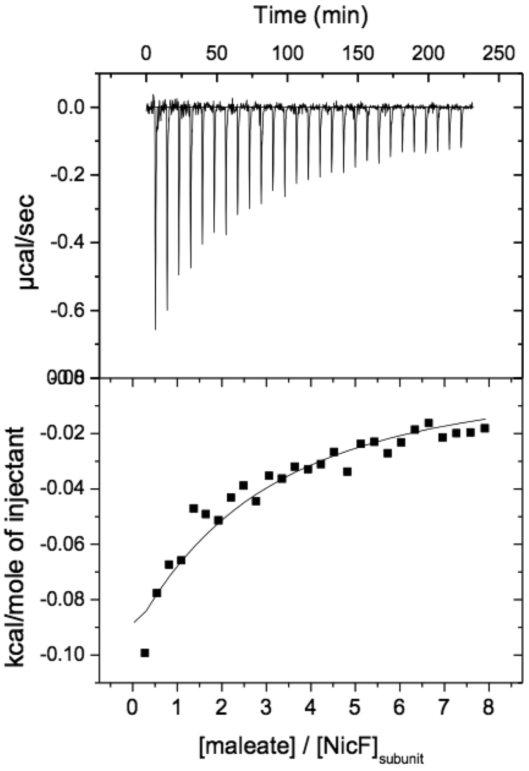

Figure 3. Calorimetric titration of NicF with maleate at 25 °C. The top plot shows the raw exothermic heats of binding, and the bottom plot shows the integrated heat vs maleate:NicF molar ratio. The fitted line is calculated assuming a one-site binding model per NicF monomer with the following thermodynamic parameters: $n = 1$, $K_D = 3.8 \pm 0.4$ mM, and $\Delta H = -0.50 \pm 0.03$ kcal/mol.

model provides an estimate for K_D of 3.8 $\pm$ 0.4 mM. In accord with this result, maleate was shown to be a competitive inhibitor of NicF with a K_I of 4.3 $\pm$ 0.4 mM (Figure S4 of the Supporting Information). From the relationships $\Delta G° = -RT \ln K_D$ and $\Delta G = \Delta H - T\Delta S$, maleate binding by NicF was observed to be accompanied by a change in entropy ($T\Delta S$) of -2.8 ± 0.3 kcal/mol at 25 °C, consistent with the typical expectation for the formation of a binary complex. If the K_M observed for maleamate in kinetic experiments (0.123 mM) approximates the K_D of the ES complex, the results from the equilibrium binding of maleate by NicF show that the enzyme has an at least ~30-fold weaker affinity for its product.

Structure of NicF. The NicF monomer is characterized by a double Rossmann-like fold (Figure 4), in which a central six-strand 3-2-1-4-5-6 parallel β-sheet is packed between two triads of α-helices. Eight monomers occupy the asymmetric unit and appear to be organized into two tetramers, one of which is shown in Figure 5. Analysis of the tetrameric structure by PISA[38] reveals a total buried surface area of ≈12000 Å^2 in the tetrameric assembly. The tetramer can also be described as a dimer of dimers of 222 symmetry with a dimerization interface (e.g., between chains A and H or B and F) characterized by a total buried surface area of ≈3900 Å^2 per dimer, and a tetramerization interface (between the two dimers) characterized by a total buried surface area of ≈4200 Å^2 (≈2100 Å^2 per pair of monomers). PISA[38] analysis suggests that NicF is tetrameric in solution, consistent with results from gel exclusion chromatography reported here.

The final structure of NicF does not contain any electron density that is consistent with the presence of zinc or other metal ions. However, the structure of NicF does contain three unusual features, all of which inhabit the putative active site of the enzyme. The first of these is a non-proline *cis*-peptide located between Ala145 and Thr146. The second is a Cys150 sulfenate (*S*-hydroxycysteine, Cso). The third is an area of triangular planar electron density that has been interpreted as acetate, which is a component of the crystallization mixture. These features are present in all eight chains of the structure and are depicted in Figure 6. The δ-oxygen of Cso150 was originally modeled as a water molecule, but the contact distance between sulfur and oxygen was too short (1.75 Å) for a water–sulfur hydrogen bond but is consistent with a covalent S–O bond. A Cso residue models well in the electron density, and an $F_c - F_o$ omit map clearly places the Cso oxygen atom within covalent bonding distance of the γ-sulfur of residue 150 (Figure 6). Cys150 is the only chemically modified Cys residue in NicF; the only other Cys residue, Cys171, is unmodified.

dx.doi.org/10.1021/bi201347n | *Biochemistry* 2012, 51, 545–554

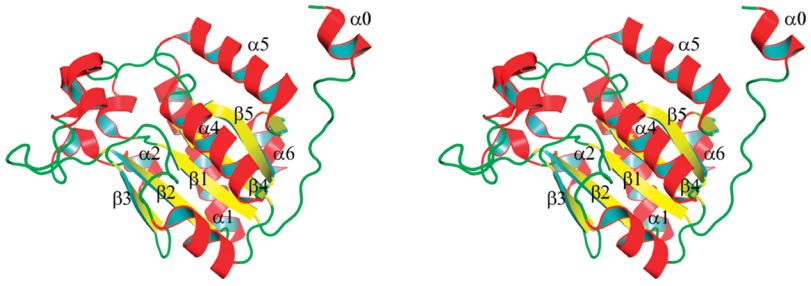

Figure 4. Cross-eyed stereo ribbon diagram of the overall fold of a single protein chain of NicF. The central core of the structure is composed of a six-strand parallel β-sheet. The β-sheet core is flanked by α-helices that pack above and below the β-sheet into a double Rossmann-like fold.

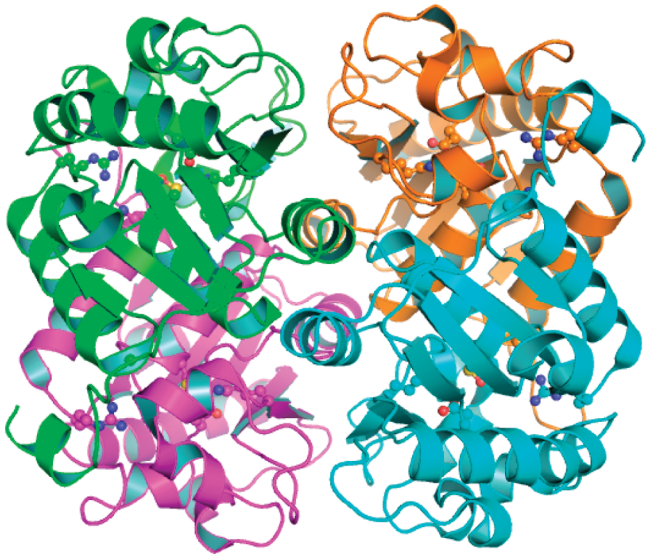

Figure 5. Ribbon diagram of the tetramer holoenzyme of NicF. Chains A, B, F, and H of PDB entry 3UAO are depicted. Each protein chain is depicted in a different color. Active site residues are depicted as balls and sticks. The dimerization interface is horizontal and the tetramerization interface vertical.

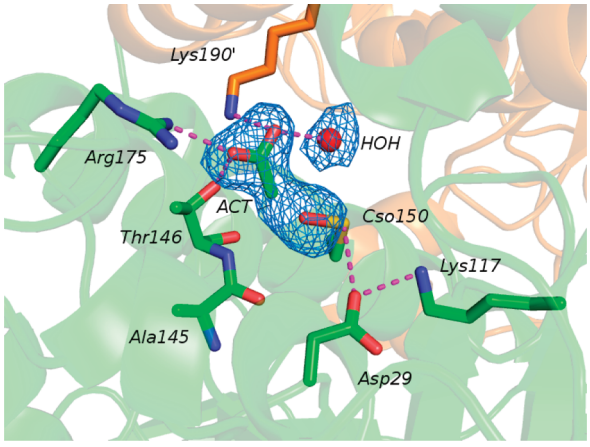

Figure 6. Putative active site of NicF. Chains A (green) and H are depicted. Key residues are depicted as sticks. Water molecule depicted as a red sphere. Likely hydrogen bonding interactions are depicted as magenta dashes. The electron density mesh depicts an $F_o - F_c$ omit map contoured at 3.0σ.

DISCUSSION

A *nic* Gene Cluster in *Bordetella*. A cluster of seven genes hypothesized to encode the enzymes of aerobic catabolism of nicotinate within *B. bronchiseptica* RB50 were identified (Figure S4 of the Supporting Information) and subsequently shown to be homologous to a functional *nic* cluster demonstrated in *P. putida*.[11] Although initial functional analyses of the recombinant forms of NicAB, NicD, NicX,[11] NicE,[39] and NicC[40] have been reported, no such detailed study has been reported for NicF from any organism, nor have the structures of any of the proteins in this pathway been determined. Obtaining a more detailed structural and functional understanding of the enzymes of this pathway has the potential for developing (1) a mechanistic understanding of biodegradation of N-heterocyclic aromatic compounds in the environment, (2) potential pharmaceutical targets in the treatment of infections by *B. pertussis* (the causative agent of whooping cough), and (3) a more complete biochemical understanding of the molecular events that effect the metabolism of $NAD^+/NADP^+$ (for a recent review, see ref 41). To this end, we began to confirm the functionality of the *nic* cluster in *Bordetella* and report here the results of our initial structural and mechanistic investigations of the *Bb*1774 gene product, which show it encodes NicF. On the basis of the findings presented here and those reported in ref 11 as well as the recent observations of NicX activity for *Bb*1773 and NicC activity for *Bb*1770 (M. J. Snider, unpublished observations), the putative *nic* cluster in *B. bronchiseptica* has probably been confirmed.

Results of kinetic analysis of purified recombinant NicF show that the enzyme achieves a physiologically relevant catalytic efficiency ($k_{cat}/K_M \sim 1 \times 10^5$ M^{-1} s^{-1} at pH 7.5 and 25 °C), matching current estimates of that measured for an "average enzyme".[42] Determination of the catalytic rate enhancement of NicF, measured by the ratio k_{cat}/k_{H_2O} (i.e., catalytic turnover compared to the rate constant for spontaneous deamination of maleamate in water), is difficult to estimate accurately. Earlier observations, from effects of pH and *N*-alkyl[43] and C=C bond alkyl substitution effects[44] on the rates of maleamate hydrolysis, suggest that nonenzymatic hydrolysis of maleamate involves intramolecular catalysis by the *cis*-carboxylate moiety and proceeds through a maleic acid anhydride intermediate. Spontaneous hydrolytic deamination of fumaramic acid, the *E* isomer of maleamate, might serve as a better model for establishing the rate of direct attack by water at the carbonyl carbon atom of the amide moiety, for which $k_{H_2O} = 1 \times 10^{-8}$ s^{-1} at 25 °C and pH 1.5.[43] As compared to this model, NicF achieves a rate enhancement of at least 10^{10}-fold. This rate enhancement is comparable to those of the other enzymes that catalyze amide bond hydrolysis[45] but probably underestimates the actual rate enhancement produced by NicF considering that the spontaneous and enzyme-catalyzed amide hydrolysis reactions proceed by different mechanisms.

dx.doi.org/10.1021/bi201347n | *Biochemistry* 2012, 51, 545–554

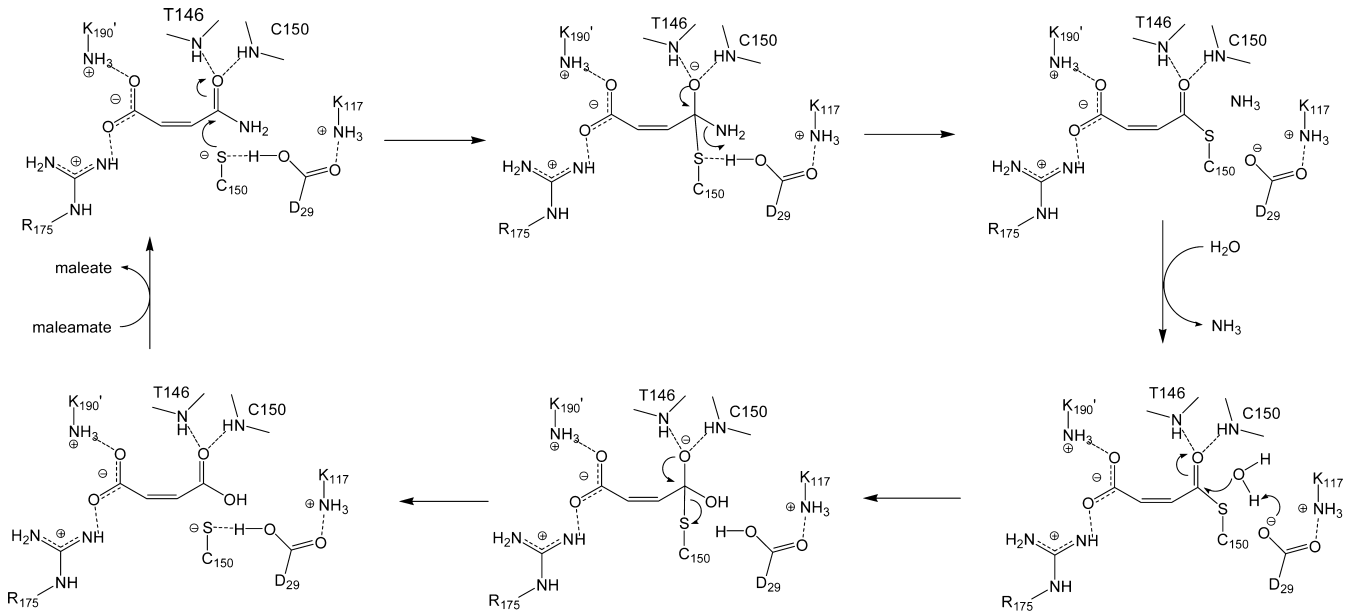

Figure 7. Proposed mechanism of maleamate hydrolysis catalyzed by NicF.

Structural Comparisons of NicF with Other Proteins. Of enzymes that have been structurally and functionally characterized, NicF shows the strongest three-dimensional homology (PDB entry, DALI[46] *Z* scores, and alignment lengths are listed in parentheses) with *Arthrobacter* sp. *N*-carbamoylsarcosine amidohydrolase (1NBA, 13.8, 194),[17] *E. coli* YcaC hydrolase[47] (1YAC, 9.7, 150), *Pyrococcus horokoshii* pyrazinamidase[18] (1IM5, 14.4, 174), and *Mycobacterium tuberculosis* pyrazinamidase[48] (3PL1, 13.0, 159). All four proteins have a non-proline *cis*-peptide bond at the same position in the protein chain: in NicF and CSHase, it is an Ala−Thr peptide bond; in the pyrazinamidases, it is an Ile−Ala (MtPZase) or Val−Ala (PhPZase) peptide bond; in YcaC, it is a Val−Val peptide bond. A common feature of this position appears to be at least one β-branched residue in the non-proline *cis*-peptide. In all but one case, the remaining residue is small (Ala). This distribution is consistent with previous data-mining studies that showed that non-proline *cis*-peptide bonds are likely to contain one β-branched residues at or near the *cis*-peptide,[49] with the most commonly occurring structural classes of residues being [Ile/Leu/Met/Val] and [Ala/Gly].[50]

Putative Active Site of NicF. The active sites of four structural homologues of NicF have been tentatively identified by the presence of conserved, and likely catalytic, residues. NicF and its homologues appear to represent a class of cysteine hydrolases characterized by a catalytic triad of residues (Cys-Asp-Lys or Cys-Asp-Arg) anchored by a Cys residue at the N-terminus of α4. The active site is in a region defined by the N-terminus of α4 and the C-termini of β2 and β1. The Cys residue is thought to act as a nucleophile in an addition−elimination mechanism of action.[17] The conserved non-proline *cis*-peptide bond is also located in this site. It is suggested that the *cis*-peptide amide and the amide nitrogen of the active site Cys residue form an oxyanion hole that stabilizes the transition state leading to the tetrahedral intermediate during hydrolysis.[18] The active sites of these hydrolases are lined with hydrophobic residues. There is some divergence from here, depending on the function of the enzyme. The pyrazinamidases contain an octahedral metal binding site within the active site region, occupied by Zn^{2+} (PhPZase) or Fe^{2+} (MtPZase), whose metal-bound water aids in the deacylation reaction during hydrolysis. In contrast, NicF and several CSHases contain basic residues (Arg and/or Lys) in this region of the active site, which is near the mouth of the active site cavity. A likely role for these basic residues is interaction with the distal carboxylate group present in both *N*-carbamoylsarcosine and maleamate, but not in pyrazinamide. Indeed, the acetate ion bound in the active site of NicF suggests that the β-OH group of Thr146, Arg175, and Lys190′ (from the neighboring protein chain) can stabilize a carboxylate moiety positioned in a region that might be expected to be occupied by the carboxylate group of maleamate bound in the active site. Key residues in the putative NicF active site are shown in Figure 6. The active site region of NicF lies along the dimerization interface, near the N-terminus of α4 and the C-terminus of α5 of the neighboring chain. Cys(Cso)150, Asp29, and Lys117 are observed within hydrogen bonding distance and likely form a "catalytic triad". The active site cavity is lined with hydrophobic residues, including Phe34, Phe40, Ile71, Met90, Leu93, Phe13′, and Try191′. At the far end of the active site, Arg175 and Lys190′ form a basic amino acid cluster. There is no evidence of a metal ion binding site in the putative active site region, nor is there any electron density visible that could be attributed to a metal ion in NicF. These structural observations are in accord with functional analyses, described above, that rule out a role for Zn^{2+}, or any other transition metal, in NicF activity. The active site cavity, which is ~4 Å in diameter and 8 Å deep, is entirely covered by the N-terminal loop of the enzyme, including helix α0′ from the neighboring chain across the dimerization interface (Figure 5). This closure of the active site cleft is also observed in CSHase, where an extended N-terminal helix from the neighboring protein chain covers the entrance to the active site cavity. Presumably, the N-terminal region of NicF must be flexible enough in solution to allow substrate access and egress of the product from the active site.

The role, if any, of the cysteine-sulfenate (Cso150) in NicF is not clear. It seems likely that the oxidation of Cys150 is an artifact of storage or crystallization conditions, neither of which

included reducing agents. Cysteine-sulfenates are well-known in enzymes, but their role is typically to act as redox centers in peroxidations or participants in redox regulation.[51] The homology of NicF with other known cysteine hydrolases does not suggest an obvious role for a cysteine-sulfenate residue. Rather, it is more likely that the active form of the enzyme contains a canonical Cys residue and that its oxidation observed here is due to its relative ease of deprotonation to the thiolate. That suggestion seems plausible considering the mechanism proposed below for NicF and is also consistent with the observation that maleate, which contains an additional negatively charged carboxylate that would be positioned near Cys150, is bound much less tightly than maleamate. Subsequent to this finding, reducing agents (DTT or TCEP) were shown to preserve enzyme activity and were included in storage buffers, providing further functional evidence of a catalytic role for a reduced thiolate.

Proposed Mechanism of Action. A mechanistic proposal for maleamate deamination catalyzed by NicF, involving a nucleophilic elimination sequence, is depicted in Figure 7. In the first step, Asp29 acts as a general base to deprotonate Cys150 for nucleophilic attack on the amide carbonyl of maleamate. [In accord with a mechanistic proposal involving the thiolate of Cys150 as a nucleophile, iodoacetamide, a thiol-specific alkylation reagent, is observed to inactivate NicF (Figure S5 of the Supporting Information).] The amide NH groups of the *cis*-peptide bond and Cys150 form an oxyanion hole to stabilize the transition state leading to the resulting tetrahedral intermediate. Asp29 acts as a general acid to protonate the amide leaving group when the tetrahedral intermediate collapses. Lys117 may serve to increase the acidity of Asp29 in this role. The deprotonated Asp29 can then act as a general base to catalyze the attack of the thioester intermediate by water, generating maleate and resetting the catalytic cycle. Although the deamination of maleamate in water proceeds efficiently through a maleic acid anhydride, the active site of NicF appears to be too small to accommodate that intermediate and is more likely poised to catalyze direct intermolecular attack of water on the thioester intermediate, as shown. Lys190′ and Arg175 likely serve to recognize the carboxylate of maleamate by electrostatic interactions and/or hydrogen bonding and orient the substrate in the active site. The structural and catalytic determinants of this mechanistic proposal are currently under active investigation.

■ ASSOCIATED CONTENT

Supporting Information

Determination of the apparent ΔH_{rxn} for maleamate hydrolysis by ITC (Figure S1), ^{1}H NMR spectra of maleamate and maleate standards for comparison with those of the reaction product of NicF (Figure S2), plot showing the decrease in UV absorbance (340 nm) as a function of time for the coupled assay for ammonia and the resulting Michaelis−Menten plot as a function of maleamate concentration (Figure S3), double-reciprocal plot of NicF activity showing competitive inhibition by maleate (Figure S4), inactivation of NicF activity by iodoacetamide measured by isothermal titration calorimetry (Figure S5), and genome analysis around the *Bb*1774 gene showing the predicted *nic* cluster in *B. bronchiseptica* (Figure S6). This material is available free of charge via the Internet at http://pubs.acs.org.

Accession Codes

Coordinates and structure factors have been deposited in the Protein Data Bank as entry 3UAO.

■ AUTHOR INFORMATION

Corresponding Author

*Telephone: (330) 263-2391. Fax: (330) 263-2386. E-mail: msnider@wooster.edu.

Funding

This research was supported in part by a Howard Hughes Medical Institute Undergraduate Science Education Program Grant at The College of Wooster, a National Science Foundation Grant to M.J.S. (CHE-0619123), and a National Science Foundation Grant to R.S.R. (CHE-0819686).

■ ACKNOWLEDGMENTS

We thank Brad Palanski for helpful comments on the manuscript.

■ ABBREVIATIONS

NicF, maleamate amidohydrolyase; CSHase, *Arthrobacter* sp. *N*-carbamoylsarcosine amidohydrolase; YcaC, *E. coli* hydrolase; PhPZase, *Pyrococcus horikoshii* pyrazinamidase; MtPZase, *M. tuberculosis* pyrazinamidase; NCS, noncrystallographic symmetry; DTT, dithiothreitol; EDTA, ethylenediaminetetraacetic acid; IPTG, isopropyl thio-β-D-galactoside; ITC, isothermal titration calorimetry; SDS−PAGE, sodium dodecyl sulfate−polyacrylamide gel electrophoresis; TCEP, tris(2-carboxyethyl)phosphine hydrochloride.

■ REFERENCES

(1) Allinson, M. J. C. (1943) A specific enzymatic method for the determination of nicotinic acid in blood. *J. Biol. Chem. 147*, 785−791.

(2) Koser, S. A., and Baird, G. R. (1944) Bacterial destruction of nicotinic acid. *J. Infect. Dis. 75*, 250−261.

(3) Pinsky, A., and Michaelis, M. (1952) The oxidation of nicotinic acid by *Pseudomonas fluorescens*. *Biochem. J. 52*, 33−38.

(4) Harary, I. (1957) Bacterial fermentation of nicotinic acid I: End products. *J. Biol. Chem. 227*, 815−822.

(5) Ensign, J. C., and Rittenberg, S. C. (1964) The pathway of nicotinic acid oxidation by a *Bacillus* species. *J. Biol. Chem. 239*, 2285−2291.

(6) Kaiser, J.-P., Feng, Y., and Bollag, J.-M. (1996) Microbial metabolism of pyridine, quinolone, acridine and their derivatives under aerobic and anaerobic conditions. *Microbiol. Rev. 60*, 483−498.

(7) Fetzner, S. (1998) Bacterial degradation of pyridine, indole, quinolone, and their derivatives under different redox conditions. *Appl. Microbiol. Biotechnol. 49*, 237−250.

(8) Harary, I. (1957) Bacterial fermentation of nicotinic acid II: Anaerbobic reversible hydroxylation of nicotinic acid to 6-hydroxynicotinic acid. *J. Biol. Chem. 227*, 823−831.

(9) Hughes, D. E. (1955) 6-Hydroxynicotinic acid as an intermediate in the oxidation of nicotinic acid by *Pseudomonas fluorescens*. *Biochem. J. 60*, 303−310.

(10) Alhapel, A., Darley, D. J., Wagener, N., Eckel, E., Elsner, N., and Pierik, A. (2006) Molecular and functional analysis of nicotinate catabolism in *Eubacterium barkeri*. *Proc. Natl. Acad. Sci. U.S.A. 103*, 12341−12346.

(11) Jimenez, J. I., Canales, A., Jimenez-Barbero, J., Ginalski, K., Rychlewski, L., Garcia, J. L., and Diaz, E. (2008) Deciphering the genetic determinants for aerobic nicotinic acid degradation: The *nic* cluster from *Pseudomonas putida* KT2440. *Proc. Natl. Acad. Sci. U.S.A. 105*, 11329−11334.

(12) Schneider, D. R., and Parker, C. D. (1982) Effect of pyridines on phenotypic properties of *Bordetella pertussis*. *Infect. Immun. 38*, 548–553.
(13) McPheat, W. L., Wardlaw, A. C., and Novotny, P. (1983) Modulation of *Bordetella pertussis* by nicotinic acid. *Infect. Immun. 41*, 516–522.
(14) Melton, A. R., and Weiss, A. A. (1993) Characterization of environmental regulators of *Bordetella pertussis*. *Infect. Immun. 61*, 807–815.
(15) Behrman, E. J., and Stanier, R. Y. (1957) The bacterial oxidation of nicotinic acid. *J. Biol. Chem. 228*, 923–945.
(16) Behrman, E. J., and Hillenbrand, E. L. (2008) Synthesis of N-formylmaleamic acid and related formylamides. *J. Chem. Res.,* 170–172.
(17) Romao, M. J., Turk, D., Gomisruth, F. X., Huber, R., Schumacher, G., Mollering, H., and Russmann, L. (1992) Crystal-structure analysis, refinement and enzymatic-reaction mechanism of N-carbamoylsarcosine amidohydrolase from *Arthrobacter* sp. at 2.0-angstrom resolution. *J. Mol. Biol. 226*, 1111–1130.
(18) Du, X. L., Wang, W. R., Kim, R., Yakota, H., Nguyen, H., and Kim, S. H. (2001) Crystal structure and mechanism of catalysis of a pyrazinamidase from *Pyrococcus horikoshii*. *Biochemistry 40*, 14166–14172.
(19) French, J. B., Cen, Y., Sauve, A. A., and Ealick, S. E. (2010) High-resolution crystal structures of *Streptococcus pneumonia* nicotinamidase with trapped intermediates provide insight into the catalytic mechanism and inhibition by aldehydes. *Biochemistry 49*, 8803–8812.
(20) Sambrook, J., Fritsch, G. F., and Maniatis, T. (1989) *Molecular Cloning: A Laboratory Guide*, Cold Spring Harbor Laboratory Press, Plainview, NY.
(21) Pace, C. N., Vajdos, F., Fee, L., Grimsley, G., and Gray, T. (1995) How to measure and predict the molar absorption-coefficient of a protein. *Protein Sci. 4*, 2411–2423.
(22) Day, N., and Keillor, J. W. (1999) A continuous spectrophotometric linked enzyme assay for transglutaminase activity. *Anal. Biochem. 274*, 141–144.
(23) Todd, M. J., and Gomez, J. (2001) Enzyme kinetics determined using calorimetry: A general assay for enzyme activity? *Anal. Biochem. 296*, 179–187.
(24) Agilent (2010) *Crysalis PRO*, Agilent Technologies Ltd., Yarnton, England.
(25) Kelley, L. A., and Sternberg, M. J. E. (2009) Protein structure prediction on the Web: A case study using the Phyre server. *Nat. Protoc. 4*, 363–371.
(26) Schrodinger, LLC (2010) *The PyMOL Molecular Graphics System*, version 1.3r1.
(27) McCoy, A. J., Grosse-Kunstleve, R. W., Adams, P. D., Winn, M. D., Storoni, L. C., and Read, R. J. (2007) Phaser crystallographic software. *J. Appl. Crystallogr. 40*, 658–674.
(28) McCoy, A. J., Grosse-Kunstleve, R. W., Storoni, L. C., and Read, R. J. (2005) Likelihood-enhanced fast translation functions. *Acta Crystallogr. D61*, 458–464.
(29) Storoni, L. C., McCoy, A. J., and Read, R. J. (2004) Likelihood-enhanced fast rotation functions. *Acta Crystallogr. D60*, 432–438.
(30) Murshudov, G. N., Vagin, A. A., and Dodson, E. J. (1997) Refinement of macromolecular structures by the maximum-likelihood method. *Acta Crystallogr. D53*, 240–255.
(31) Stein, N. (2008) CHAINSAW: A program for mutating pdb files used as templates in molecular replacement. *J. Appl. Crystallogr. 41*, 641–643.
(32) Cowtan, K. (2010) Recent developments in classical density modification. *Acta Crystallogr. D66*, 470–478.
(33) Cowtan, K. (2006) The Buccaneer software for automated model building. 1. Tracing protein chains. *Acta Crystallogr. D62*, 1002–1011.
(34) Emsley, P., and Cowtan, K. (2004) Coot: Model-building tools for molecular graphics. *Acta Crystallogr. D60*, 2126–2132.
(35) Winn, M. D., Isupov, M. N., and Murshudov, G. N. (2001) Use of TLS parameters to model anisotropic displacements in macromolecular refinement. *Acta Crystallogr. D57*, 122–133.
(36) Winn, M. D., Murshudov, G. N., and Papiz, M. Z. (2003) Macromolecular TLS refinement in REFMAC at moderate resolutions. *Methods Enzymol. 374*, 300–321.
(37) Luo, H.-B., Zheng, H., Zimmerman, M. D., Chruszcz, M., Skarina, T., Egorova, O., Savchenko, A., Edwards, A. M., and Minor, W. (2010) Crystal structure and molecular modeling study of N-carbamoylsarcosine amidase Ta0454 from *Thermoplasma acidophilum*. *J. Struct. Biol. 169*, 304–311.
(38) Krissinel, E., and Henrick, K. (2007) Inference of macromolecular assemblies from crystalline state. *J. Mol. Biol. 372*, 774–797.
(39) Hatakeyama, K., Asia, Y., Uchida, Y., Kobayashi, M., Teresawa, M., and Yukawa, H. (1997) Gene cloning and characterization of maleate *cis-trans* isomerase from *Alcaligenes faecalis*. *Biochem. Biophys. Res. Commun. 239*, 74–79.
(40) Nakano, H., Wieser, M., Hurth, B., Yoshida, T., Yamane, T., and Nagasawa, T. (1999) Purification, characterization and gene cloning of 6-hydroxynicotinate 3-monooxygenase from *Pseudomonas fluorescens* TN5. *Eur. J. Biochem. 260*, 120–126.
(41) Sauve, A. A. (2008) NAD^+ and vitamin B_3: From metabolism to therapies. *J. Pharmacol. Exp. Ther. 324*, 883–893.
(42) Bar-Even, A., Noor, E., Savir, Y., Liebermeister, W., Davidi, D., Tawfik, D. S., and Milo, R. (2011) The moderately efficient enzyme: Evolutionary and physicochemical trends shaping enzyme parameters. *Biochemistry 50*, 4402–4410.
(43) Dahlgren, G., and Simmerman, N. L. (1965) The effect of ethyl substitution on the kinetics of the hydrolysis of maleamic and phthalamic acid. *J. Phys. Chem. 69*, 3626–3630.
(44) Kirby, A. J., and Lancaster, P. W. (1972) Structure and efficiency in intramolecular and enzymic catalysis. Catalysis of amide hydrolysis by the carboxy-group of substituted maleamic acids. *J. Chem. Soc., Perkin Trans. 2*, 1206–1214.
(45) Wolfenden, R. (2006) Degrees of difficulty of water consuming reactions in the absence of enzymes. *Chem. Rev. 106*, 3379–3396.
(46) Holm, L., and Rosenström, P. (2010) Dali server: Conservation mapping in 3D. *Nucleic Acids Res. 38*, W545–W549.
(47) Colovos, C., Cascio, D., and Yeates, T. O. (1998) The 1.8 angstrom crystal structure of the ycaC gene product from *Escherichia coli* reveals an octameric hydrolase of unknown specificity. *Struct. Folding Des. 6*, 1329–1337.
(48) Petrella, S., Gelus-Ziental, N., Maudry, A., Laurans, C., Boudjelloul, R., and Sougakoff, W. (2011) Crystal Structure of the Pyrazinamidase of *Mycobacterium tuberculosis*: Insights into Natural and Acquired Resistance to Pyrazinamide. *PLoS One 6*, No. e15785.
(49) Pal, D., and Chakrabarti, P. (1999) Cis Peptide Bonds in Proteins: Residues Involved, Their Conformations, Interactions and Locations. *J. Mol. Biol. 294*, 271–288.
(50) Exarchos, K. P., Exarchos, T. P., Rigas, G., Papaloukas, C., and Fotiadis, D. I. (2011) Extraction of consensus protein patterns in regions containing non-proline cis peptide bonds and their functional assessment. *BMC Bioinf. 12*, 142.
(51) Claiborne, A., Yeh, J. I., Mallett, T. C., Luba, J., Crane, E. J. III, Charrier, V., and Parsonage, D. (1999) Protein-Sulfenic Acids: Diverse Roles for an Unlikely Player in Enzyme Catalysis and Redox Regulation. *Biochemistry 38*, 15407–15416.
(52) Engh, R. A., and Huber, R. (1991) Accurate bond and angle parameters for X-ray protein structure refinement. *Acta Crystallogr. A47*, 392–400.
(53) Chen, V. B., Arendall, W. B., Headd, J. J., Keedy, D. A., Immormino, R. M., Kapral, G. J., Murray, L. W., Richardson, J. S., and Richardson, D. C. (2010) MolProbity: All-atom structure validation for macromolecular crystallography. *Acta Crystallogr. D66*, 12–21.